Journal of Fluids & Structure (2002) **16**(6), 795–809
doi:10.1006/jfls.446 available online at http://www.idealibrary.com on IDEAL®

VIBRATIONS OF CIRCULAR CYLINDRICAL SHELLS WITH NONUNIFORM CONSTRAINTS, ELASTIC BED AND ADDED MASS. PART III: STEADY VISCOUS EFFECTS ON SHELLS CONVEYING FLUID

M. Amabili and R. Garziera

Dipartimento di Ingegneria Industriale, Università di Parma
Parco Area delle Scienze 181/A, Parma I – 43100, Italy

(Received 19 March 2001; received in revised form 17 October 2001)

The effect of steady viscous forces on vibrations of shells with internal and annular flow has been considered by using the time-mean Navier–Stokes equations. The model developed in Part I of the present study, capable of simulating shells with nonuniform boundary conditions, added masses and partial elastic bed, has been extended to include nonuniform prestress. The effect of steady viscous forces has been added to the inviscid flow formulation considered in Part II of the present study. A computer code, DIVA, has been constructed by using the model developed in this series of papers. It has been validated by comparison with available results for shells with uniform constraints and has been used to study shells with nonuniform constraints and added lumped masses.

1. INTRODUCTION

Vibrations of empty and fluid-filled shells with nonuniform boundary conditions and additional complications (added masses and partial elastic bed) have been studied in Part I of the present study (Amabili & Garziera 2000). The problem has been extended in Part II (Amabili & Garziera 2002) to consider pressurized shells in contact with internal, external and annular ideal flows. The ideal flow considered is inviscid, irrotational and incompressible. This third part concludes the study by considering the effect of steady viscous effects of the flowing fluid on the shell vibrations.

Païdoussis *et al*. (1985, 1991) investigated the steady viscous effects on vibrations and stability of clamped and cantilevered circular shells with internal and annular flow by using the time-mean Navier–Stokes equations. They concluded that the effect of viscosity is stabilizing for internal flow and destabilizing for annular flow. This result is mainly due to the fact that the numerical analyses were performed by keeping constant the value of the outlet pressure (by giving the inlet pressure necessary to reach the outlet pressure required). As a consequence of the pressure drop, an additional triangular pressure distribution is applied to the shell in the case of viscous flow. This pressure is internal, therefore stabilizing, for internal flow and destabilizing for external annular flow. Païdoussis *et al*. (1985, 1991) also found that the effect of viscosity was more pronounced for annular flow than for internal flow.

0889-9746/02/060795 + 15 $35.00/0

El Chebair *et al.* (1990) and Nguyen *et al.* (1994) investigated the effect of unsteady viscous forces, which represent the time-dependent fluid viscous forces, for circular cylindrical shells with internal and annular flow. In particular, El Chebair *et al.* (1990) used the linearized Navier–Stokes equation to obtain the unsteady viscous forces for incompressible viscous flow for simply supported shells. The solution was obtained analytically; some difficulties were found in applying the no-slip condition at the shell wall. As discussed by Nguyen *et al.* (1994), this solution was not completely satisfactory. For this reason, Nguyen *et al.* (1994) used a CFD-based model to study stability of cantilevered shells considering unsteady viscous forces. The finite-difference-based, time-marching technique with artificial compressibility was used to solve the linearized, unsteady Navier–Stokes equations. They found that unsteady viscous effects tend to be reduced with diminishing annular gap width, provided that the gap is sufficiently small.

In the present study, the effect of steady viscous forces on vibrations of shell with internal and annular flows has been considered by using the time-mean Navier–Stokes equations. As observed by El Chebair *et al.* (1990), this effect is more important than the effect of unsteady viscous forces. The model developed in Part I of the present study (Amabili & Garziera 2000), capable of simulating shells with nonuniform boundary conditions, added masses and partial elastic bed, has been extended to include nonuniform prestress. The effect of steady viscous forces has been added to the inviscid flow formulation considered in Part II (Amabili & Garziera 2001). A computer code, DIVA, has been developed by using the model developed in this series of papers. It has been validated by comparison with available results for shells with uniform constraints and has been used to study shells with nonuniform constraints and added lumped masses.

2. POTENTIAL ENERGY ASSOCIATED WITH MEMBRANE NONUNIFORM PRESTRESS

Similar to Parts I and II of the present study (Amabili & Garziera 2000, 2001), a circular cylindrical shell of length L, radius R and thickness h is considered. The cylindrical coordinates x, r, θ are used with origin on the upstream shell base. The displacements of the shell mean surface are indicated with u, v, w in the axial, circumferential and radial directions, respectively. The additional strain energy stored by the shell during vibration under membrane prestress is given by (e.g., Leissa 1973)

$$\begin{aligned} V_P &= \int_0^{2\pi}\int_0^L\int_{-h/2}^{h/2} \left(\sigma_x\varepsilon_x + \sigma_\theta\varepsilon_\theta + \tau_{x\theta}\,\gamma_{x\theta}\right) \mathrm{d}x\, R\,\mathrm{d}\theta\,\mathrm{d}z \\ &= \int_0^{2\pi}\int_0^L \left(N_x\varepsilon_x + N_\theta\varepsilon_\theta + N_{x\theta}\,\gamma_{x\theta}\right) \mathrm{d}x\, R\,\mathrm{d}\theta, \end{aligned} \tag{1}$$

where N_x, N_θ and $N_{x\theta}$ are the membrane forces per unit length, in axial, circumferential and tangential directions, respectively, ε_x, ε_θ and $\gamma_{x\theta}$ are the strains in axial, circumferential and tangential directions, respectively, and σ_x, σ_θ and $\tau_{x\theta}$ are the corresponding stresses. In equation (1), only the second-order terms of the nonlinear strain-displacement equations must be used (e.g., Soedel 1993). The linear part is used to find the stress resultants necessary to evaluate the membrane forces per unit length. In equation (1), the membrane forces due to vibrations have been neglected with respect to the initial prestress; this is necessary to retain linear equations of motion [see, e.g., Soedel (1993)].

Different nonlinear strain–displacement equations can be used according to different nonlinear shell theories. By using the Sanders–Koiter nonlinear shell theory, these

relationships are (e.g. Leissa 1973; Yamaki 1984; Selmane & Lakis 1997)

$$\varepsilon_x = \frac{\partial u}{\partial x} + \frac{1}{2}\left(\frac{\partial w}{\partial x}\right)^2 + \frac{1}{8}\left(\frac{\partial v}{\partial x} - \frac{\partial u}{R\,\partial\theta}\right)^2, \tag{2a}$$

$$\varepsilon_\theta = \frac{\partial v}{R\,\partial\theta} + \frac{w}{R} + \frac{1}{2}\left(-\frac{\partial w}{R\,\partial\theta} + \frac{v}{R}\right)^2 + \frac{1}{8}\left(\frac{\partial u}{R\,\partial\theta} - \frac{\partial v}{\partial x}\right)^2, \tag{2b}$$

$$\gamma_{x\theta} = \frac{\partial u}{R\partial\theta} + \frac{\partial v}{\partial x} - \frac{\partial w}{\partial x}\left(\frac{v}{R} - \frac{\partial w}{R\,\partial\theta}\right). \tag{2c}$$

Substituting the second-order parts of equations (2) into equation (1), the additional potential energy of the shell due to nonuniform prestress is obtained. The additional stiffness matrix of the system is obtained by using the expansion of shell displacements introduced in Parts I and II (Amabili & Garziera 2000, 2001)

$$\left\{\begin{array}{c} u \\ v \\ w \end{array}\right\}_S = \sum_{n=0}^{\infty}\sum_{m=1}^{\infty}\sum_{j=1}^{3} a_{nmj} \left\{\begin{array}{c} A_{nmj}\cos(n\theta)\cos(m\pi x/L) \\ B_{nmj}\sin(n\theta)\sin(m\pi x/L) \\ \cos(n\theta)\sin(m\pi x/L) \end{array}\right\} \tag{3a}$$

for symmetric modes with respect to $\theta = 0$, and

$$\left\{\begin{array}{c} u \\ v \\ w \end{array}\right\}_A = \sum_{n=1}^{\infty}\sum_{m=1}^{\infty}\sum_{j=1}^{3} b_{nmj} \left\{\begin{array}{c} A_{nmj}\sin(n\theta)\cos(m\pi x/L) \\ B_{nmj}\cos(n\theta)\sin(m\pi x/L) \\ \sin(n\theta)\sin(m\pi x/L) \end{array}\right\} \tag{3b}$$

for antisymmetric modes with respect to $\theta = 0$, and the expressions of the membrane forces per unit length. The membrane forces for the particular case of nonuniform prestress due to viscous flow are evaluated in the next section. In equation (3a) and (3b), n is the number of circumferential waves, m is the number of axial half-waves, and $j = 1, 2, 3$ indicates the modes with prevalent radial, circumferential and longitudinal displacements, respectively.

3. STEADY LOADS FOR FULLY DEVELOPED TURBULENT FLOW

In case of fully developed turbulent, incompressible axial flow inside or outside a shell, it is possible to evaluate the steady loads by using the time-mean Navier–Stokes equations (Laufer 1953)

$$\frac{1}{\rho_F}\frac{\partial P}{\partial x} = -\frac{1}{r}\frac{\mathrm{d}}{\mathrm{d}r}(r\,\overline{u_x u_r}) + \frac{\eta}{r}\frac{\mathrm{d}}{\mathrm{d}r}\left(r\frac{\mathrm{d}U}{\mathrm{d}r}\right), \tag{4a}$$

$$\frac{1}{\rho_F}\frac{\partial P}{\partial r} = -\frac{1}{r}\frac{\mathrm{d}}{\mathrm{d}r}(r\,\overline{u_r^2}) + \frac{\overline{u_\theta^2}}{r}, \tag{4b}$$

$$0 = \frac{\mathrm{d}}{\mathrm{d}r}(\overline{u_r u_\theta}) + 2\frac{\overline{u_r u_\theta}}{r}, \tag{4c}$$

where ($\bar{}$) is the time-mean, ρ_F is the fluid mass-density, η is the kinematic viscosity and u_x, u_θ, u_r are the fluctuating velocities in axial, angular and radial directions, respectively. Long mathematical manipulations are required to obtain the results of interest for internal

flow (Païdoussis *et al.* 1985, 1991), namely,

$$P(x,r) = -2\frac{\rho_F}{R}U_\tau^2 x - \rho_F\overline{u_r^2} + \rho_F\int_R^r \frac{\overline{u_\theta^2} - \overline{u_r^2}}{r}\,\mathrm{d}r + P(0,R), \tag{5}$$

$$U_\tau = \left(-\eta\frac{\mathrm{d}U}{\mathrm{d}r}\right)_{r=R}^{1/2} = (\tau_W/\rho_F)^{1/2} = \left(\frac{1}{8}fU^2\right)^{1/2}, \tag{6}$$

where U is the mean axial flow velocity, U_τ is the so-called stress velocity, τ_w is the fluid frictional force per unit area on the shell, and f is the friction factor.

For external and annular flows, the solutions of the time-mean Navier–Stokes equations are (Païdoussis *et al.*, 1985, 1991)

$$P(x,r) = -2\frac{R_1}{R_1^2 - r_m^2}\rho_F U_\tau^2 x - \rho_F\overline{u_r^2} + \rho_F\int_R^r \frac{\overline{u_\theta^2} - \overline{u_r^2}}{r}\,\mathrm{d}r + P(0,R), \tag{7}$$

$$U_\tau = \left(-\eta\frac{\mathrm{d}U}{\mathrm{d}r}\right)_{r=R}^{1/2} = (\tau_W/\rho_F)^{1/2} = \left(\frac{1}{8}\frac{R_1^2 - r_m^2}{R_1(R_1 - R)}fU^2\right)^{1/2}, \tag{8}$$

where R_1 is the radius of the outer rigid cylinder delimiting the flow (eventually $R_1 \to \infty$ for unbounded external flow) and r_m is the radius at which the mean velocity U is maximum. The value of r_m cannot be analytically obtained. However, the experiments of Brighton & Jones (1964) showed that if $R/R_1 \geqslant 0{\cdot}8$, r_m can be approximated by its counterpart in case of laminar flow, i.e.,

$$r_m = \left[\frac{R_1^2 - R^2}{2\ln(R_1/R)}\right]^{1/2}. \tag{9}$$

On the shell surface, a particularly simple expression is obtained from equation (5)

$$P(x,R) = -2\frac{\rho_F}{R}U_\tau^2 x + P(0,R). \tag{10}$$

The pressure drop in the shell is

$$P(0,R) - P(L,R) = 2\frac{\rho_F}{R}U_\tau^2 L = \frac{\rho_F}{4R}LfU^2.$$

Similarly, equation (7) evaluated at $r = R$ becomes

$$P(x,R) = -2\frac{R_1}{R_1^2 - r_m^2}\rho_F U_\tau^2 x + P(0,R), \tag{11}$$

where P now is external with respect to the shell, and the pressure drop is

$$P(0,R) - P(L,R) = \frac{\rho_F}{4(R_1 - R)}LfU^2.$$

Essentially, equation (10) can be considered as a special case of equation (11) where the radius delimiting externally the fluid domain is $R_1 = R$ and $r_m = 0$.

The friction factor f in equations (6) and (8) can be calculated by using the experimental Colebrook equation

$$\frac{1}{\sqrt{f}} + 2\log_{10}\left(\frac{\delta/(2R)}{3{\cdot}7} + \frac{2{\cdot}51}{\mathrm{Re}\sqrt{f}}\right) = 0, \tag{12}$$

where δ is the average height of surface imperfections of the shell surface and Re is the Reynolds number. In particular, $\mathrm{Re} = 2RU/\eta$ for internal flow, $\mathrm{Re} = 2(R_1 - R)U/\eta$ for external annular flow and $2(R_1 - R)$ is the equivalent hydraulic diameter for annular flow. The root of equation (12) can easily be found numerically.

The effect of steady viscous forces on shell dynamics consists of (i) a constant distributed axial load applied to the shell surface and (ii) a radial pressure exerted by the fluid on the shell, which is linearly decreasing with x, as shown by equations (6) and (10) and equations (8) and (11) for internal and external flows, respectively. In particular, for both internal and external flows, the constant axial force per unit area is given by

$$\tau_w = \rho_F U_\tau^2. \tag{13}$$

and the radial pressure is given by equation (10) or (11) for internal or external flow, respectively.

The force per unit length in angular direction is given by

$$N_\theta = \begin{cases} R\left(P_0 - 2\dfrac{\rho_F}{R}U_\tau^2 x\right) & \text{for internal flow,} \\ -R\left(P_0 - 2\rho_F \dfrac{R_1}{R_1^2 - r_m^2}U_\tau^2 x\right) & \text{for external flow,} \end{cases} \tag{14}$$

where P_0 is the pressure at $x = 0$ (entrance pressure) on the shell wall. The average force per unit length in angular direction is $\bar{N}_\theta = R(P_0 - \rho_F L U_\tau^2/R)$ for internal flow and $\bar{N}_\theta = -R\left[P_0 - \rho_F R_1 L U_\tau^2/(R_1^2 - r_m^2)\right]$ for external annular flow.

For equilibrium and congruence, the force per unit length in axial direction is given by

$$N_x = \begin{cases} \rho_F U_\tau^2(\tfrac{1}{2}L - x) + (k_{\mathrm{eq}}/k_S)\nu R\left(P_0 - \dfrac{\rho_F}{R}U_\tau^2 L\right) & \text{for internal flow} \\ \rho_F U_\tau^2(\tfrac{1}{2}L - x) + (k_{\mathrm{eq}}/k_S)\nu R\left(P_0 - \rho_F \dfrac{R_1}{R_1^2 - r_m^2}U_\tau^2 L\right) & \text{for external flow} \end{cases} \tag{15}$$

where ν is Poisson ratio, $k_S = 2\pi RhE/L$ is the axial stiffness of the shell, $k_{\mathrm{eq}} = 1/(1/k_1 + 1/k_S + 1/k_2)$ and $k_1 = \int_0^{2\pi} \tilde{k}_0(\theta)\, R\, \mathrm{d}\theta = 2\pi R\tilde{k}_{0,0}$ and $k_2 = \int_0^{2\pi} \tilde{k}_L(\theta)\, R\, \mathrm{d}\theta = 2\pi R\tilde{k}_{L,0}$ are the axial stiffnesses of the elastic constraints at $x = 0$, L, respectively, as computed in Appendix A of Part II of the present study (Amabili & Garziera 2001). In equation (15), the contribution of $\bar{N}_\theta$ to the shell contraction in axial direction has been considered and the two axial forces necessary at the shell ends for equilibrium have been considered equal in magnitude.

4. POTENTIAL ENERGY DUE TO VISCOUS FORCES

The constant forces per unit length due to uniform pressurization of shells have already been investigated in Part II of the present study. Only the effect of viscous steady forces is investigated here. In particular, the case of internal flow is analysed since the case of external flow is immediately obtained as a particular case, as shown in the previous section.

The forces per unit length to be inserted in equation (1) are

$$N_x = \rho_F U_\tau^2\left\{[\tfrac{1}{2} - \nu(k_{\mathrm{eq}}/k_S)]L - x\right\}, \quad N_\theta = -\rho_F U_\tau^2 2x \quad N_{x\theta} = 0 \tag{16a–c}$$

The potential energy V_V stored by the shell during vibrations under initial prestress due to viscous forces is given by

$$V_V = \frac{1}{2}\int_0^{2\pi}\int_0^L \left\{ N_x\left[\frac{1}{2}\left(\frac{\partial w}{\partial x}\right)^2 + \frac{1}{8}\left(\frac{\partial v}{\partial x} - \frac{\partial u}{R\,\partial\theta}\right)^2\right] + N_\theta\left[\frac{1}{2}\left(-\frac{\partial w}{R\,\partial\theta} + \frac{v}{R}\right)^2 + \frac{1}{8}\left(\frac{\partial u}{R\,\partial\theta} - \frac{\partial v}{\partial x}\right)^2\right]\right\} \mathrm{d}x\, R\,\mathrm{d}\theta. \tag{17}$$

In equation (17), the Sanders–Koiter nonlinear shell theory has been used to obtain the second-order strain–displacement relationships, see equations (2). After mathematical manipulations of equation (17), the following expression is obtained for symmetric modes:

$$V_V = \rho_F U_\tau^2 R\pi \sum_{n,s=0}^{\infty}\sum_{m,i=1}^{\infty}\sum_{j,\tilde{j}=1}^{3} a_{nmj}a_{si\tilde{j}}\varsigma_n\delta_{n,s}\left\{\left[\frac{1}{2} - \nu\frac{k_{\mathrm{eq}}}{k_s}\right]L\delta_{m,i}\delta_{j,\tilde{j}}\left[\frac{m^2\pi^2}{4L} + B_{nmj}^2\frac{m^2\pi^2}{16L} + A_{nmj}^2\frac{n^2L}{16R^2} + A_{nmj}A_{si\tilde{j}}\frac{nm\pi}{8R}\right] - \gamma_{mi}\left[\frac{mi\pi^2}{4L^2}\left(2 + \frac{3}{2}B_{nmj}B_{si\tilde{j}}\right) + \frac{3}{8}\frac{n^2}{R^2}A_{nmj}\,A_{si\tilde{j}} + \frac{3n\pi}{8LR}(iA_{nmj}B_{si\tilde{j}} + mA_{si\tilde{j}}B_{nmj})\right] - \frac{\beta_{mi}}{R^2}\left[n^2 + B_{si\tilde{j}}n + B_{nmj}s + B_{nmj}B_{si\tilde{j}}\right]\right\}, \tag{18a}$$

where $\delta_{n,s}$ is the Kronecker delta, $\varsigma_n = 2$ *if* $n = 0$, and $\varsigma_n = 1$ *if* $n > 0$.

$$\gamma_{mi} = \int_0^L x\cos(m\pi x/L)\cos(i\pi x/L)\,\mathrm{d}x = \begin{cases} L^2/4 & \text{if } i = m, \\ \dfrac{L^2[-(i^2+m^2) + (i^2+m^2)(-1)^m(-1)^i]}{(i\text{-}m)^2(i+m)^2\pi^2} & \text{if } i \neq m, \end{cases}$$

and

$$\beta_{mi} = \int_0^L x\sin(m\pi x/L)\sin(i\pi x/L)\,\mathrm{d}x = \begin{cases} L^2/4 & \text{if } i = m, \\ \dfrac{2miL^2[-1 + (-1)^m(-1)^i]}{(i\text{-}m)^2(i+m)^2\pi^2} & \text{if } i \neq m. \end{cases}$$

For antisymmetric modes, equation (18a) is modified into

$$V_V = \rho_F U_\tau^2 R\pi \sum_{n,s=1}^{\infty}\sum_{m,i=1}^{\infty}\sum_{j,\tilde{j}=1}^{3} b_{nmj}b_{s,i,\tilde{j}}\varsigma_n\delta_{n,s}\left\{\left[\frac{1}{2} - \nu\frac{k_{\mathrm{eq}}}{k_s}\right]L\delta_{m,i}\delta_{j,\tilde{j}}\left[\frac{m^2\pi^2}{4L} + B_{nmj}^2\frac{m^2\pi^2}{16L} + A_{nmj}^2\frac{n^2L}{16R^2} + A_{nmj}A_{si\tilde{j}}\frac{nm\pi}{8R}\right] - \gamma_{mi}\left[\frac{mi\pi^2}{4L^2}\left(2 + \frac{3}{2}B_{nmj}B_{si\tilde{j}}\right) + \frac{3}{8}\frac{n^2}{R^2}A_{nmj}A_{si\tilde{j}} - \frac{3n\pi}{8LR}(iA_{nmj}B_{si\tilde{j}} + mA_{si\tilde{j}}B_{nmj})\right] - \frac{\beta_{mi}}{R^2}\left[n^2 - B_{si\tilde{j}}n - B_{nmj}s + B_{nmj}B_{si\tilde{j}}\right]\right\}. \tag{18b}$$

In case of nonuniform prestress due to a different load with respect to viscous forces, the approach is similar.

5. STIFFNESS MATRIX DUE TO VISCOUS FORCES

Only a finite number of modes in the Rayleigh–Ritz expansion are retained. The three-dimensional matrix $\mathbf{q}$ of the Ritz coefficients is introduced

$$q_{nmj} = \begin{cases} a_{nmj} & \text{for symmetric modes,} \quad n = 0, \ldots N-1; \quad m = 1, \ldots, \tilde{N}; \quad j = 1,2,3, \\ b_{nmj} & \text{for antisymmetric modes,} \quad n = 1, \ldots N; \quad m = 1, \ldots, \tilde{N}; \quad j = 1,2,3. \end{cases} \tag{19}$$

In equation (19), the expansion of symmetric and antisymmetric modes involves $3 \times N \times \tilde{N}$ terms. The potential energy associated with initial prestress due to viscous forces can be written as

$$V_V = \frac{1}{2} R \mathbf{q}^T \mathbf{K}_V \mathbf{q}, \tag{20}$$

where

$$\begin{aligned} (\mathbf{K}_V)_{nsmij\tilde{j}} = 2\rho_F U_\tau^2 \pi \varsigma_n \delta_{n,s} \Bigg\{ & \left[\frac{1}{2} - v\frac{k_{\text{eq}}}{k_s}\right] L \delta_{m,i} \delta_{j,\tilde{j}} \left[\frac{m^2\pi^2}{4L} + B_{nmj}^2 \frac{m^2\pi^2}{16L}\right. \\ & \left. + A_{nmj}^2 \frac{n^2 L}{16R^2} + A_{nmj} A_{si\tilde{j}} \frac{nm\pi}{8R}\right] - \gamma_{mi} \left[\frac{mi\pi^2}{4L^2}\left(2 + \frac{3}{2} B_{nmj} B_{si\tilde{j}}\right) + \frac{3}{8}\frac{n^2}{R^2} A_{nmj} A_{si\tilde{j}}\right. \\ & \left. + \frac{3n\pi}{8LR}(iA_{nmj} B_{si\tilde{j}} + mA_{si\tilde{j}} B_{nmj})\right] - \frac{\beta_{mi}}{R^2}[n^2 + B_{si\tilde{j}} n + B_{nmj} s + B_{nmj} B_{si\tilde{j}}]\Bigg\} \end{aligned} \tag{21a}$$

for symmetric modes, and

$$\begin{aligned} (\mathbf{K}_V)_{nsmij\tilde{j}} = 2\rho_F U_\tau^2 \pi \varsigma_n \delta_{n,s} \Bigg\{ & \left[\frac{1}{2} - v\frac{k_{\text{eq}}}{k_s}\right] L \delta_{m,i} \delta_{j,\tilde{j}} \left[\frac{m^2\pi^2}{4L} + B_{nmj}^2 \frac{m^2\pi^2}{16L}\right. \\ & \left. + A_{nmj}^2 \frac{n^2 L}{16R^2} + A_{nmj} A_{si\tilde{j}} \frac{nm\pi}{8R}\right] - \gamma_{mi} \left[\frac{mi\pi^2}{4L^2}\left(2 + \frac{3}{2} B_{nmj} B_{si\tilde{j}}\right) + \frac{3}{8}\frac{n^2}{R^2} A_{nmj} A_{si\tilde{j}}\right. \\ & \left. - \frac{3n\pi}{8LR}(iA_{nmj} B_{si\tilde{j}} + mA_{si\tilde{j}} B_{nmj})\right] - \frac{\beta_{mi}}{R^2}[n^2 - B_{si\tilde{j}} n - B_{nmj} s + B_{nmj} B_{si\tilde{j}}]\Bigg\} \end{aligned} \tag{21b}$$

for antisymmetric modes.

6. NUMERICAL RESULTS

Numerical results have been obtained by using the computer code DIVA (Amabili & Garziera 2001) where steady viscous loads have been included. Calculations have been performed to (i) validate the computer code by comparison with available results for shells with uniform constraints; (ii) to show the convergence of the method by increasing the number of terms in the Ritz expansion; (iii) to study shells clamped at some points around the edges and otherwise simply supported (riveted shells); (iv) to investigate the effects of steady viscous loads; and (v) to study shells with lumped masses; this configuration is of interest in some applications.

6.1. Validation and Convergence

The computer code has been validated by analysing a circular cylindrical shell, clamped at the ends, and having the following characteristics: $R = 0{\cdot}0909\,\text{m}$, $L = 1\,\text{m}$, $h = 0{\cdot}5\,\text{mm}$, $E = 206 \times 10^9\,\text{Pa}$, $\rho = 7\,800\,\text{kg/m}^3$, $\rho_F = 1\,000\,\text{kg/m}^3$ and $v = 0{\cdot}3$. The shell is assumed to have zero internal roughness, contains flowing water with the kinematic viscosity

$1{\cdot}2 \times 10^{-6}\,\mathrm{m}^2/\mathrm{s}$ and is immersed in external still water delimited by an external radius of $R_1 = 0{\cdot}1\,\mathrm{m}$. The same case was previously studied by Païdoussis *et al.* (1985) for modes with three circumferential waves ($n = 3$) by using a model with three longitudinal modes and by assuming rigid baffles outside the shell length instead of a flexible shell as in the present model. Both present calculations and results of Païdoussis *et al.* (1985) have been obtained by keeping the outlet pressure (downstream) equal to zero and giving the required value to the inlet pressure (upstream), as calculated by using the Colebrook equation (12). A nondimensional fluid velocity V is introduced for convenience, defined as in Païdoussis *et al.* (1985) by $V = U/\{E/[\rho_S(1-\nu^2)]\}^{1/2}$, U being the dimensional velocity; similarly, a non-dimensional, frequency Ω is defined as $\Omega = \Lambda R/\{E/[\rho_S(1-\nu^2)]\}^{1/2}$, Λ being the corresponding circular frequency.

A comparison of results obtained with the computer code DIVA and by Païdoussis *et al.* (1985) is given in Figure 1. The agreement between the curve (Païdoussis *et al.* 1985) and the points (present results) is sufficiently good, partially excluding the third mode. Differences can be attributed mainly to the different boundary conditions for the liquid outside the shell length used in the two studies, and secondarily to the different numbers of modes used in the expansion of the shell displacement. Present results have been obtained by using 3×20 longitudinal modes in the Ritz expansion (20 is the maximum number of longitudinal half-waves) given by equation (3), and the stiffnesses of the axial and rotational distributed springs used to simulate clamped ends are $\tilde{k} = 10^9\,\mathrm{N/m}^2$ and $c = 10^8\,\mathrm{N/m}$, respectively.

Figure 2 shows the results obtained for the same case by retaining 3×40 modes in the expansion of the shell displacement; results obtained with 3×20 modes, as given in Figure 1, are also shown for comparison. This figure proves that the first and second modes practically reached convergence with 20 longitudinal modes of the simply supported shell; for higher modes, more terms are needed. However, the difference in the results obtained with 20 and 40 modes is small for all the modes shown in Figure 2.

A comparison of results obtained with 3×20 modes for viscous and inviscid flow is given in Figure 3. It is clearly shown that the frequencies of free vibration decrease much

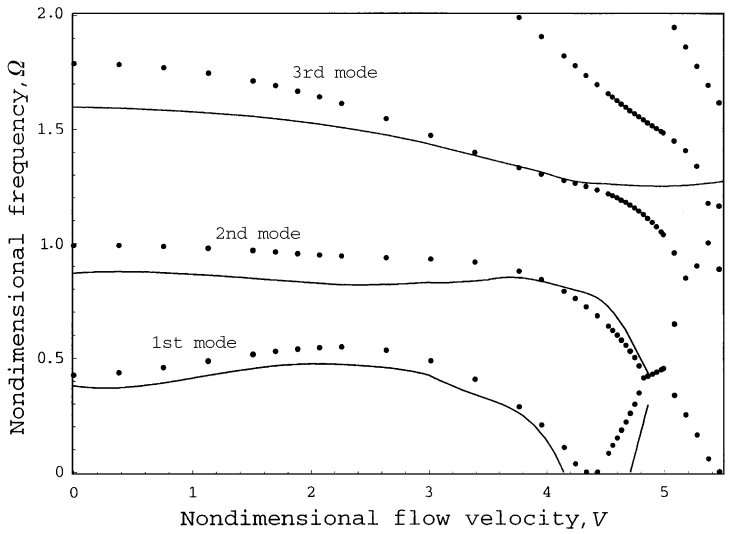

Figure 1. Nondimensional frequencies of free vibration Ω of a clamped shell conveying water versus nondimensional flow velocity; calculations for zero outlet pressure; modes with $n = 3$ and the nondimensionalization scheme of Païdoussis *et al.* (1985): —, results from Païdoussis *et al.* (1985); ●, present results.

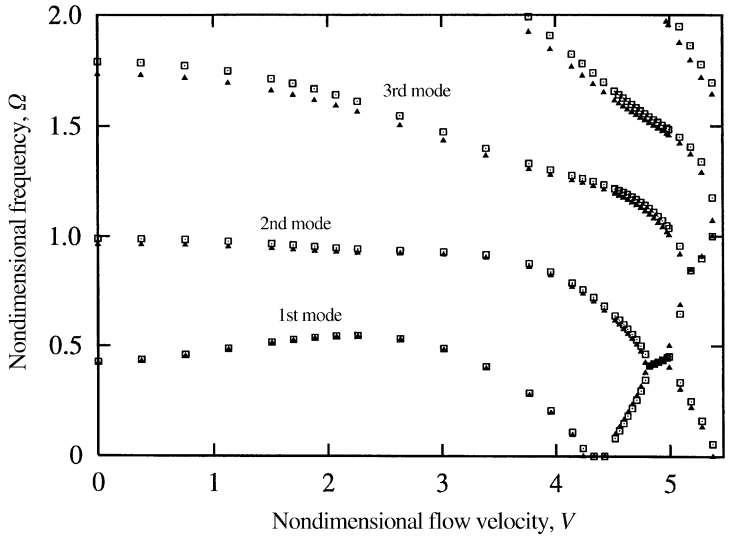

Figure 2. Nondimensional frequencies of free vibration Ω of clamped shell conveying water versus nondimensional flow velocity; calculations for zero outlet pressure; modes with $n = 3$ and the nondimensionalization scheme of Païdoussis *et al.* (1985): □, present results with 3×20 longitudinal modes; ▲, present results with 3×40 longitudinal modes.

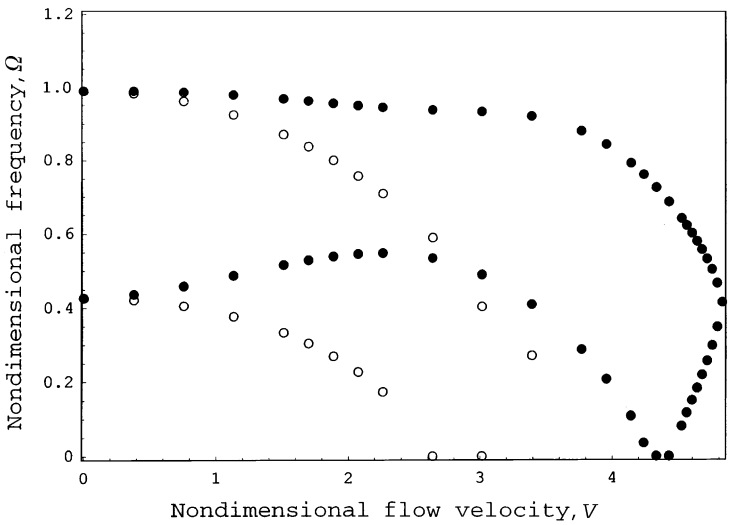

Figure 3. Nondimensional frequencies of free vibration Ω of clamped shell conveying water versus nondimensional flow velocity; calculations for zero outlet pressure; modes with $n = 3$ and the nondimensionalization scheme of Païdoussis *et al.* (1985): ●, viscous flow; ○, inviscid flow.

more with flow velocity for inviscid flow. However, it must be considered that calculations have been made by keeping the outlet pressure constant. It means that, for viscous flow, the inlet pressure becomes larger by increasing the flow velocity with respect to the inviscid case. This result is discussed in more detail in Section 6.3.

6.2. Riveted Shell (Simply Supported Shell With Clamped Points)

The case analysed here was studied by Amabili & Garziera (2001) by considering inviscid flow. It considers a circular cylindrical shell containing flowing water and having the following characteristics: $L/R = 2$, $h/R = 0{\cdot}01$, $L = 1\,\text{m}$, $E = 206 \times 10^9\,\text{Pa}$, $\rho = 7\,850\,\text{kg/m}^3$, $\rho_F = 1000\,\text{kg/m}^3$ and $\nu = 0{\cdot}3$. Kinematic viscosity $1{\cdot}2 \times 10^{-6}\,\text{m}^2/\text{s}$ and internal roughness (average height of internal surface imperfections) of the shell of $0{\cdot}8\,\mu\text{m}$ are assumed. A nondimensional fluid velocity V is introduced for convenience, defined as in Weaver & Unny (1973) by $V = U/\{(\pi^2/L)[D/(\rho\, h)]^{1/2}\}$, with $D = Eh^3/[12(1-\nu^2)]$; similarly, a nondimensional, generally complex, frequency Ω is defined as $\Omega = \Lambda/\{(\pi^2/L^2)[D/(\rho h)]^{1/2}\}$, Λ being the corresponding circular frequency. Nonuniform boundary conditions are assumed to be around the shell ends, as in the case of riveted shell. In particular, four equispaced clamped arcs, simulating rivets, of an angular amplitude of $3{\cdot}5^\circ$ are considered at each shell end. These arcs are symmetrically distributed with respect to the origin $\theta = 0$ and away from this point; both slope in the axial direction and axial displacements are restrained at the rivet location by using springs of very high stiffness ($\tilde{k} = 10^{10}\,\text{N/m}^2$ and $c = 10^{10}\,\text{N/m}$) simulating rigid constraints. Outside these clamped arcs, the shell is simply supported. In the Ritz expansion, $3 \times 20 \times 10$ modes are used, where 20 is the maximum number of circumferential waves and 10 is the maximum number of longitudinal half-waves.

Figure 4 gives the nondimensional frequencies of free vibration of the shell versus the non-dimensional fluid velocity V for both symmetric modes (with respect to $\theta = 0$), see Figure 4(a), and antisymmetric modes, see Figure 4(b). Calculations have been performed by keeping the outlet pressure (downstream) equal to zero and giving the required value to the inlet pressure (upstream). These results are compared with those obtained for the same unpressurized shell containing inviscid flow (Amabili & Garziera 2001) and it shows that steady viscous effects slightly increase the shell stability. This is explained by the pressurization given for viscous flow at the inlet shell end to exceed the friction and to have zero pressure at the outlet shell end; this gives a triangular pressure along the shell length. However, in the inviscid case, zero pressure acts on the shell.

6.3. Effect of Steady Viscous Loads

Free vibrations of an aluminium circular cylindrical shell, simply supported at the ends, containing flowing water have been studied. Two identical axial forces are assumed at the shell ends to guarantee equilibrium in axial direction. The shell has the following characteristics: $R = 0{\cdot}041275\,\text{m}$, $L = 0{\cdot}1206\,\text{m}$, $h = 0{\cdot}127\,\text{mm}$, $E = 70 \times 10^9\,\text{Pa}$, $\rho = 2700\,\text{kg/m}^3$, $\rho_F = 1000\,\text{kg/m}^3$ and $\nu = 0{\cdot}33$. The shell contains flowing water and is immersed in external still water delimited by an external radius $R_1 = 0{\cdot}103\,\text{m}$. Kinematic viscosity $1{\cdot}2 \times 10^{-6}\,\text{m}^2/\text{s}$ and internal roughness of the shell of $0{\cdot}8\,\mu\text{m}$ are assumed. In contrast with previous cases, a constant inlet pressure of 7×10^4 Pa is taken; and a constant external pressure of $7{\cdot}6135 \times 10^4$ Pa is assumed to act outside the shell. Here, $3 \times 8 \times 10$ modes are used in the Ritz expansion, where 8 is the maximum number of circumferential waves and 10 is the maximum number of longitudinal half-waves.

Figure 5 shows the frequencies of free vibration for the modes with $n = 5$, 6, 7 circumferential waves versus the flow velocity for both cases of viscous and inviscid flows. The fundamental mode has $n = 6$ circumferential waves; the second mode has $n = 7$ circumferential waves. In this case, unsteady viscous loads significantly reduce both frequencies and stability. As a consequence of keeping the inlet pressure constant, the effect of viscous loads is that of decreasing the internal pressure along the shell. Therefore,

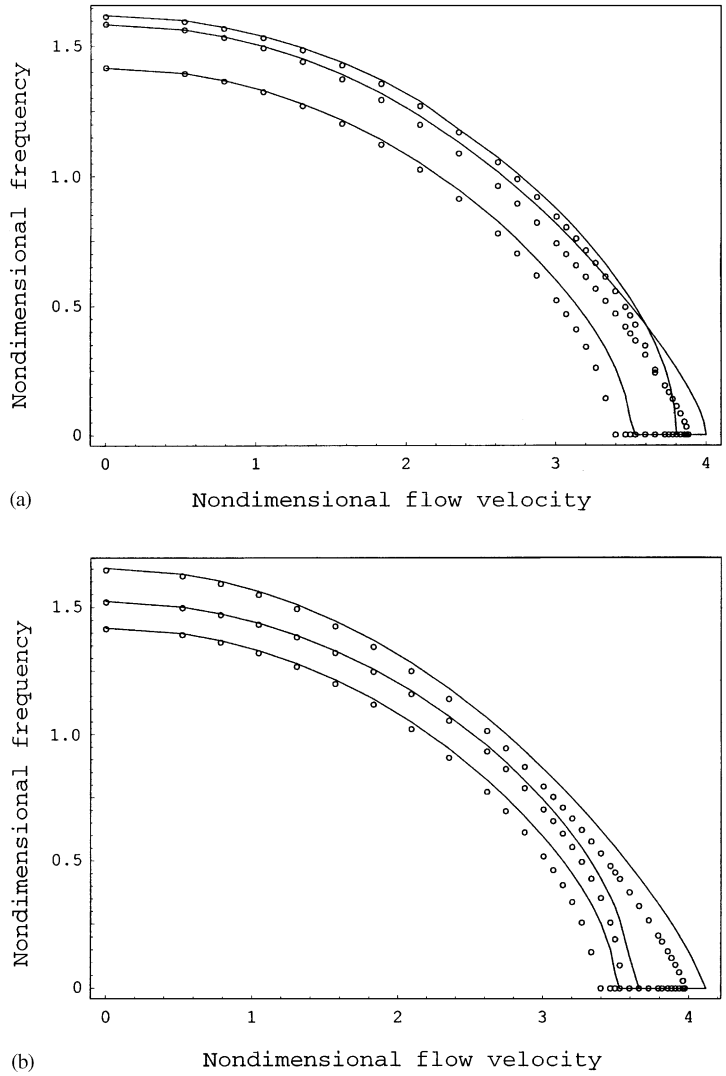

Figure 4. First three nondimensional frequencies of free vibration Ω for the shell with four rivets conveying water versus nondimensional flow velocity; nondimensionalization scheme of Weaver & Unny (1973); calculations for zero outlet pressure: —, viscous flow; ○, inviscid flow. (a) Symmetric modes; and (b) antisymmetric modes.

the effect seems to be the opposite of that previously found for the riveted shell in Section 6.2. Steady viscous forces in the flow give a triangular pressure distribution along the shell and, secondarily, give an axial load. The triangular pressure diagram and the axial load have a significant effect on the shell dynamics for sufficiently high flow velocities. The effect of viscous loads can be considered stabilizing if compared with results for a shell conveying inviscid flow, computed for the same outlet pressure; the contrary is obtained if comparison is made with results computed for shells having the same inlet pressure. Moreover, the effect of viscosity is much more significant in Figs. 3 and 5 than in Figure 4. In fact, the effect of viscous loads is more important for very thin and long shells than for thicker and shorter shells, as the one analysed in Figure 4. For longer shells, the pressure

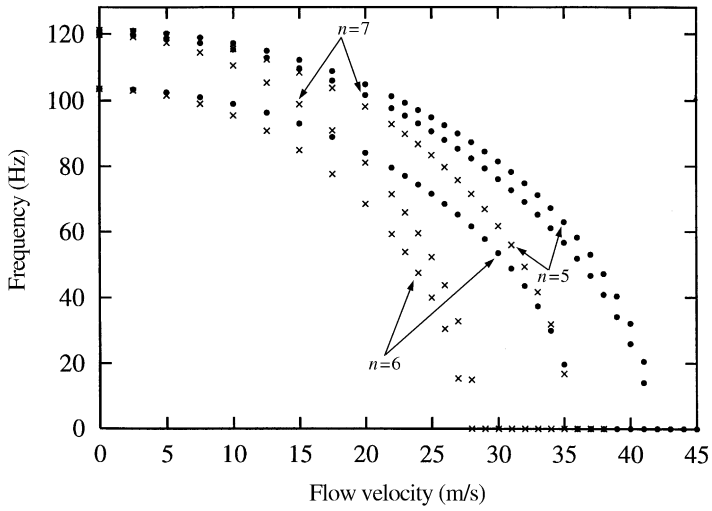

Figure 5. First three frequencies of free vibration for a simply supported aluminium shell versus flow velocity; calculations for a constant inlet pressure of 7×10^4 Pa: ●, inviscid flow; ×, viscous flow.

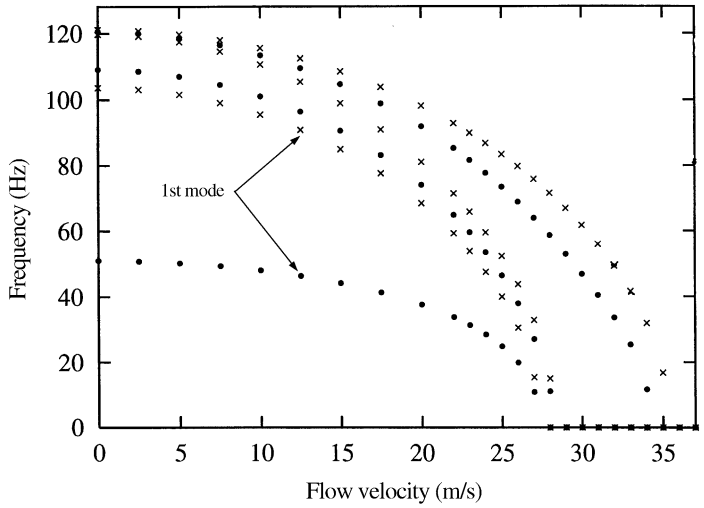

Figure 6. First three frequencies of free vibration for a simply supported aluminium shell versus flow velocity; calculations for constant inlet pressure of 7×10^4 Pa: ●, shell with three masses; ×, shell without masses.

drop is larger, and for thinner shells the effect of pressure on the shell dynamics is more important than for thicker shells.

6.4. Shell with Lumped Masses

The same case studied in Section 6.3 is considered here with the addition of three lumped masses of 50 g located at the same angular coordinate $\theta = 0$ and at axial coordinate $x = L/4$, $L/2$ and $3L/4$. The modes $3 \times 10 \times 12$ are used in the Ritz expansion, where 10 is the maximum number of circumferential waves and 12 is the maximum number of longitudinal half-waves. Figure 6 shows the frequencies of free vibration of the first three

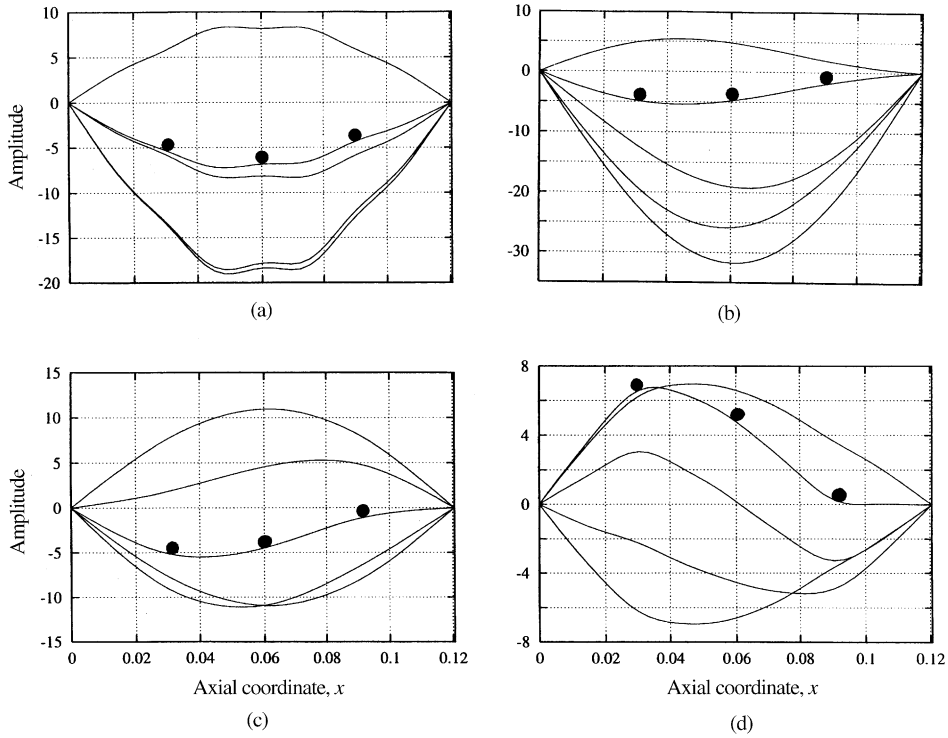

Figure 7. Complex mode shapes (in a radial section) of a simply supported aluminium shell with three masses for flow velocity $U = 15$ m/s at five consecutive instants, with time difference $T/8$ (T is the vibration period); points locate the lumped masses. (a) First mode, 44·1 Hz; (b) second mode, 90·5 Hz; (c) third mode, 104·6 Hz; and (d) fourth mode, 115·4 Hz.

symmetric modes (with respect to $\theta = 0$) in case of viscous flow. The same shell without masses is also shown for comparison. The presence of the lumped masses largely decreases the fundamental frequency but has a much smaller effect on the second and third eigenfrequencies.

Figure 7 shows the radial displacement w of the shell with the three masses for a flow velocity of 15 m/s. The first four symmetric, complex modes are represented in a radial shell section at $\theta = 0$ and are plotted in five different instants in order to show the evolution of the shape in a vibration period. The corresponding three-dimensional mode shapes, plotted at instant $t = 0$, are shown in Figure 8. In particular, Figure 7(a) shows that the shape of the fundamental mode is largely modified by the lumped masses with respect to the one of the shell without masses.

7. CONCLUSIONS

This paper concludes the series of three papers on vibrations of shells with nonuniform constraints, added masses, elastic bed and prestress conveying or immersed in annular axial flow. The computer code DIVA has been developed in order to include many complications by adding opportune stiffness and mass matrices. In particular, in the present, Part III of the study, the effect of steady viscous forces has been investigated. Steady viscous effects in the flow give a triangular pressure distribution along the shell and,

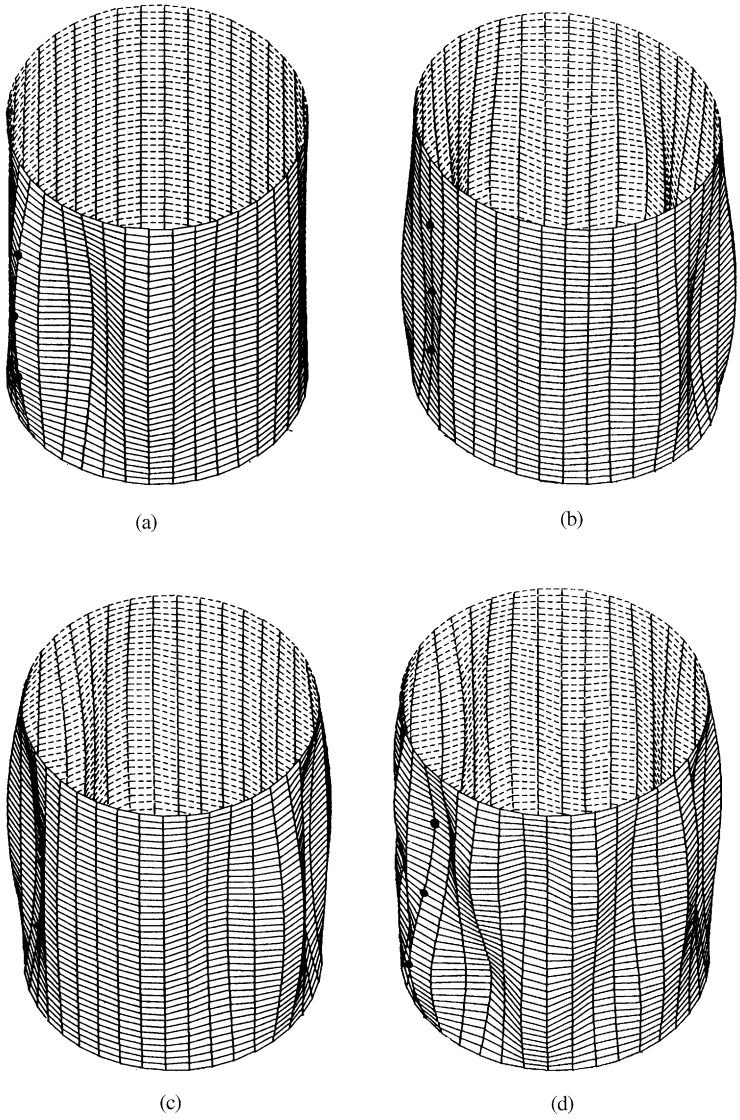

Figure 8. Mode shapes for flow velocity $U = 15$ m/s at instant $t = 0$; points locate the lumped masses. (a) First mode, 44·1 Hz; (b) second mode, 90·5 Hz; (c) third mode, 104·6 Hz; (d) fourth mode, 115·4 Hz.

secondarily, give an axial load. The effect of viscous loads can be considered stabilizing if compared with results computed for shells conveying inviscid flow having the same outlet pressure; the contrary is obtained if comparison is made with results computed for shells having the same inlet pressure.

References

Amabili, M. & Garziera, R. 2000 Vibrations of circular cylindrical shells with nonuniform constraints, elastic bed and added mass; Part I: empty and fluid-filled shells. *Journal of Fluids and Structures* **14,** 669–690.

Amabili, M. & Garziera, R. 2002 Vibrations of circular cylindrical shells with nonuniform constraints, elastic bed and added mass; Part II: shells containing or immersed in axial flow. *Journal of Fluids and Structures* **16**, 31–51.

Brighton, J. A. & Jones, J. B. 1966 Fully developed turbulent flow in annuli. *ASME Journal of Basic Engineering* **86**, 835–844.

El-Chebair, A., Misra, A. K. & Païdoussis, M. P. 1990 Theoretical study of the effect of unsteady viscous forces on inner- and annular-flow-induced instabilities of cylindrical shells. *Journal of Sound and Vibration* **138**, 457–478.

Laufer, J. 1953 The structure of turbulence in fully developed pipe flow. NACA Technical Note 2954.

Leissa, A. W. 1973 *Vibration of Shells*, NASA SP-288. Washington, DC: Government Printing Office. Now available from The Acoustical Society of America, 1993.

Nguyen, V. B., Misra, A. K. & Païdoussis, M. P. 1994 A CFD-based model for the study of the stability of cantilevered coaxial cylindrical shells conveying viscous fluid. *Journal of Sound and Vibration* **176**, 105–125.

Païdoussis, M. P., Misra, A. K. & Chan, S. P. 1985 Dynamics and stability of coaxial cylindrical shells conveying viscous fluid. *Journal of Applied Mechanics* **52**, 389–396.

Païdoussis, M. P., Nguyen, V. B., & Misra, A. K. 1991 A theoretical study of stability of cantilevered coaxial cylindrical shells conveying fluid. *Journal of Fluids and Structures* **5**, 127–164.

Selmane, A. & Lakis, A. A. 1997 Non-linear dynamic analysis of orthotropic open cylindrical shells subjected to a flowing fluid. *Journal of Sound and Vibration* **202**, 67–93.

Soedel, W. 1993 *Vibrations of Shells and Plates*. New York: Marcel Dekker.

Weaver, D. S. & Unny, T. E. 1973 On the dynamic stability of fluid-conveying pipes. *Journal of Applied Mechanics* **40**, 48–52.

Yamaki, N. 1984 *Elastic Stability of Circular Cylindrical Shells*. Amsterdam: North-Holland.